Energy & Environmental Science

Accepted Manuscript

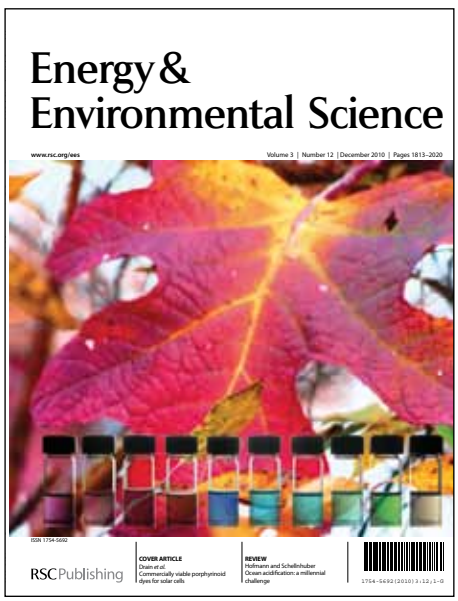

This is an *Accepted Manuscript*, which has been through the RSC Publishing peer review process and has been accepted for publication.

Accepted Manuscripts are published online shortly after acceptance, which is prior to technical editing, formatting and proof reading. This free service from RSC Publishing allows authors to make their results available to the community, in citable form, before publication of the edited article. This *Accepted Manuscript* will be replaced by the edited and formatted *Advance Article* as soon as this is available.

To cite this manuscript please use its permanent Digital Object Identifier (DOI®), which is identical for all formats of publication.

More information about *Accepted Manuscripts* can be found in the **Information for Authors**.

Please note that technical editing may introduce minor changes to the text and/or graphics contained in the manuscript submitted by the author(s) which may alter content, and that the standard **Terms & Conditions** and the **ethical guidelines** that apply to the journal are still applicable. In no event shall the RSC be held responsible for any errors or omissions in these *Accepted Manuscript* manuscripts or any consequences arising from the use of any information contained in them.

Light harvesting vesicular donor–acceptor scaffold limits the rate of charge recombination in the presence of an electron donor

*Rijo T. Cheriya, Ajith R. Mallia and Mahesh Hariharan**

School of Chemistry, Indian Institute of Science Education and Research Thiruvananthapuram, CET Campus, Sreekaryam, Thiruvananthapuram, Kerala, INDIA 695 016

† Electronic supplementary information (ESI) available: Light harvesting vesicular donor–acceptor scaffold limits the rate of charge recombination in the presence of an electron donor. See DOI:

We report the synthesis and excited state properties of single component light harvesting donor-acceptor dyad **(*R*/*S*)-NP(OH)$_2$** containing α,β-dihydroxypropyl side-chain that can undergo molecule-bilayer-vesicle-gel-crystal transition. By virtue of steric hindrance offered by orthogonal naphthalimide and 2,6-diisopropylphenyl substituents, a very weak H-type excitonic interactions between the perylenimide units resulted in high fluorescence quantum yield in the dyad based metastable vesicular gel having a near-quantitative excitation energy transfer from naphthalimide to perylenimide. Femtosecond transient absorption measurements of the dyad **(*R*/*S*)-NP(OH)$_2$**:indole co-gel exhibit the vesicular scaffold promoted extension of the survival

time of charge separated states (~1.4 ns) when compared to ultrafast charge recombination (~6 ps) in dyad **(*R*/*S*)-NP(OH)$_2$**:indole solution.

Broader context

Energy as well as electron transfer processes in self-assembled systems are crucial in the development of artificial light harvesting and solar cell based functional materials. Existing non–covalent donor–acceptor containing self-assembled light harvesting systems lack control on i) stoichiometry, ii) orientation and iii) distance between the constituent donor and acceptor units that can limit the efficiency of excitation energy transfer. We choose perylenimide-naphthalimide chromophoric array for the present study, known to be a potential and stable material in photonic devices. Our present finding offers efficient excitation energy transfer in covalently linked donor-acceptor dyads in a self-assembled vesicular gel and photoinduced electron transfer properties in the presence of external electron donor (indole) co-gel that could help in designing artificial light harvesting/photonic devices having better energy followed by charge transport properties.

Introduction

Excitation energy and electron transfer processes in crowded environments are vital for natural[1-4]/artificial[5-7] photosynthesis and photonic applications.[8-12] Such processes in isolated donor–acceptor (D–A) systems still possess immense interest.[13] Non-covalent D–A pairs that exhibit efficient light harvesting and favorable excited-state properties in the condensed media such as amorphous, thin film,[14] vesicle,[15-18] gel,[19-22] liquid crystal[23] and crystalline[24] state received recent attention. Despite being efficient in light-harvesting and colour-tunable properties,[19-21, 25] the major limitations in D–A co-assemblies is the control[26] of i) stoichiometry, ii) distance and iii)

orientation between the donor and the acceptor units. Excitation energy transfer in self-assembled covalent D–A dyads that includes amorphous,[27] thin film,[28, 29] crystal[27, 30, 31] and liquid crystalline state[32] received less attention. Dearth of literature reports in light harvesting self-assembled covalent D–A dyads could be due to the strong propensity of the aromatic surface[33] to self-assemble[34, 35] and subsequent exciton interactions[36-38]/electron transfer[39-42] that could alter the excited state properties. By virtue of curvature properties,[43] vesicular scaffolds[44, 45] could be superior for light harvesting processes similar to the chromatophoric vesicular assembly in the natural photosynthetic unit.[46] A single molecular D–A dyad that can assemble to form vesicles/gel and retain favourable excited state properties could be a potential scaffold for light harvesting applications. Concurrently, Wasielewski and co-workers have pioneered in covalent D–A pairs that can undergo photoinduced electron transfer in aggregates extending the lifetime of charge-separated intermediates.[42, 47, 48] However, combination of light harvesting and charge separation in self-assembled architectures received limited attention.[41, 49] We demonstrate that vesicular scaffold of a covalent D–A antenna can efficiently harvest light and can undergo photoinduced energy followed by electron transfer in the presence of an electron donor.

We recently reported efficient excitation energy transfer in near-orthogonal naphthalimide (donor)–perylenimide (acceptor) dyad **NP(OH)** in solution and crystalline state (Fig. 1).[31, 50] A subtle modification of the dyad using **(*R/S*)**-α,β-dihydroxypropyl side-chain imparted optimal amphiphilicity to promote the formation of a **(*R/S*)-NP(OH)$_2$** based vesicular gel in 1:2 dichloromethane (DCM)/hexane mixture that allowed us to investigate the photoinduced processes of covalent D–A pair in the gel state. To the best of our knowledge, this is the first report of a covalent D–A vesicle/gel that possesses efficient 'Forster-type' light harvesting properties resulting in orange–red fluorescence (λ_{em} = 584 nm) and high-fluorescence

quantum yield (Φ_f = 54%). The vesicular gel of **(*R*/*S*)-NP(OH)$_2$** exhibits stability in the presence of an electron donor (indole) making the dyad–donor co-gel, a potential candidate for combining efficient light harvesting and charge separation properties.

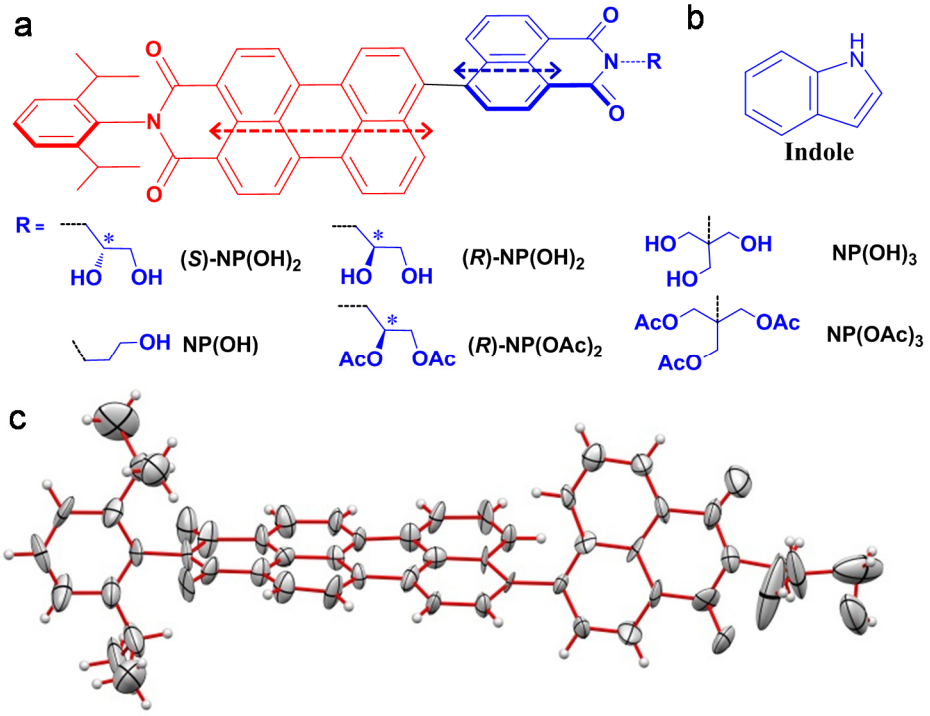

Fig. 1 Chemical structure of the molecules under investigation and the crystal structure of the dyad **(*R*)-NP(OH)$_2$**. Molecular structure of (a) the dyads **NP(OH)**, **(*R*/*S*)-NP(OH)$_2$**, **(*R*)-NP(OAc)$_2$**, **NP(OH)$_3$**, **NP(OAc)$_3$**, arrows indicate the orientation of the transition dipole moment of the naphthalimide (**NI**) and perylenimide (**PI**) units; (b) indole (electron donor) and (c) single crystal X-ray structure of the dyad **(*R*)- NP(OH)$_2$** (See CIF).

Results

The dyads **(*R*/*S*)-NP(OH)$_2$** were synthesised through Stille coupling between tributyltin derivative of perylenimide and 4-bromo-N-**(*R*/*S*)**-2,3-dihydroxypropyl naphthalimide (Scheme S1†).[50, 51] Monohydroxy **NP(OH)**,[50, 51] trihydroxy **NP(OH)$_3$** and protected analogues **NP(OAc)$_2$** and **NP(OAc)$_3$** of the dyad, having different degrees of amphiphilicity, were also synthesised (Scheme S1–S2†). UV–Vis absorbance of dyad **(*R*)-NP(OH)$_2$** (Fig. 2a) in DCM could be described as sum of the absorbance of naphthalimide (**NI**) centred at 340 nm and perylenimide

(**PI**) centred at 480 nm indicating that **(*R*)-NP(OH)$_2$** behaves as individual chromophores though connected by a covalent bond (Fig. S1†). X-ray structure (Fig. 1c), cyclic voltammetry and photophysical studies of the dyad **(*R*)-NP(OH)$_2$** and structurally analogous **NP(OH)**[50] indicated

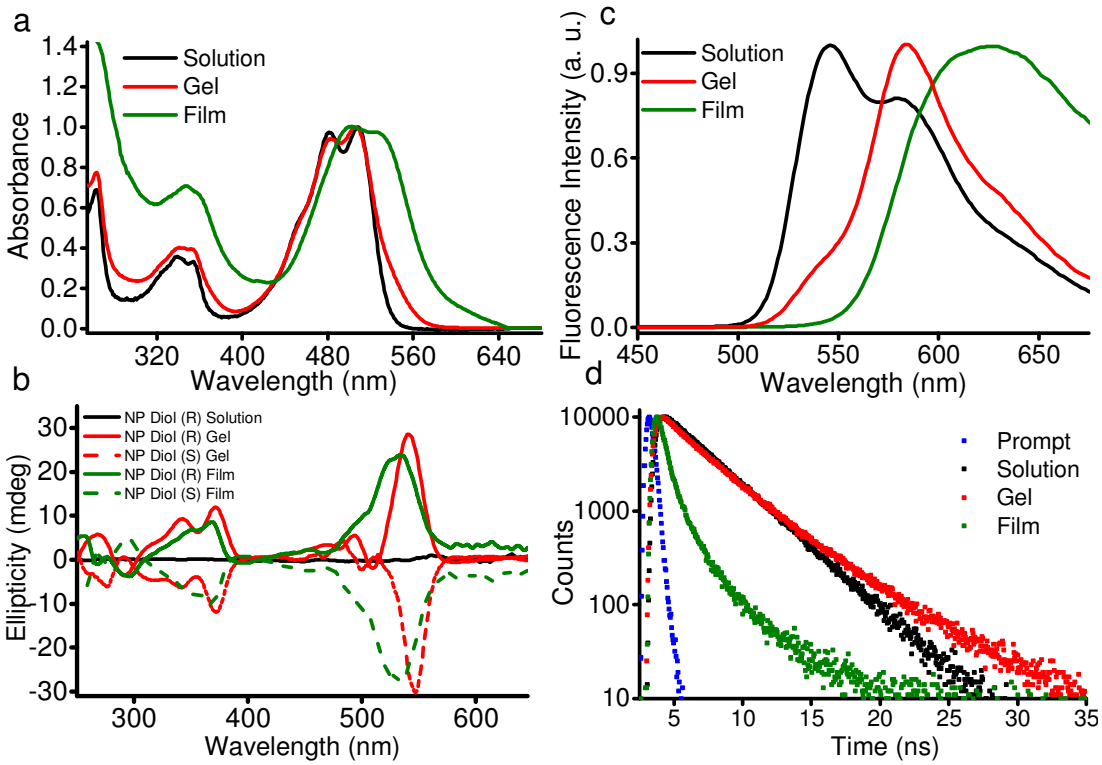

Fig. 2 Light harvesting and chiroptical properties of dyad **NP(OH)$_2$** in solution, gel and film state. (a) UV–Vis absorption spectra; (b) CD spectra; (c) fluorescence spectra (λ_{ex} = 345 nm) and (d) time-resolved fluorescence decay of **(*R*)-NP(OH)$_2$** in DCM [black], **(*R*)-NP(OH)$_2$** gel in DCM:hexane (1:2) mixture [red], **(*R*)-NP(OH)$_2$** thin film [green] and prompt [blue] when excited at 340 nm and emission collected at 550 nm (solution) and 580 nm (gel and film). **(*S*)-NP(OH)$_2$** gel [dashed red] and thin film [dashed green] only for CD spectra.

near-orthogonal arrangement and negligible orbital interactions between constituent naphthalimide and perylenimide units. Absence of circular dichroism (CD) signal (Fig. 2b) corresponding to **NI/PI** units indicates the presence of equal amounts of mutually enantiomeric atropisomers[52, 53] of the **(*R*/*S*)-NP(OH)$_2$** in DCM (Fig. S2†), consistent with both the axially chiral forms (1:1) in the unit cell. Upon direct excitation of the **PI** unit at 475 nm, **(*R*)-NP(OH)$_2$** in DCM exhibited fluorescence emission (Φ_f = 0.75 ± 0.04) centred at 546 nm having a shoulder

at 580 nm corresponding to the **PI** unit (Fig. S3†). Upon excitation at 345 nm, efficient energy transfer[54] from singlet excited state of **NI** to **PI** unit of **(*R*)-NP(OH)$_2$** in DCM resulted in the **PI** emission centered at 546 nm (Fig. 2c). Time-resolved fluorescence of **(*R*)-NP(OH)$_2$** in DCM exhibited mono-exponential decay having a lifetime of 3.7 ns, when excited at 340 nm (Fig. 2d) and 439 nm (Fig. S4a, b†). Increasing volume fraction of hexane in a solution of **(*R*)-NP(OH)$_2$** in DCM showed a blue-shift of 5 nm and a systematic decrease in the UV–Vis absorbance centred at 513 nm with the formation of a band around 560 nm (Fig. S5†). Upon excitation at 345 nm, observed significant quenching and blue-shift in the **PI** emission of **(*R*)-NP(OH)$_2$** at lower DCM:hexane ratio could be attributed to H-type perylenimide aggregates in **(*R*)-NP(OH)$_2$**. Orthogonally arranged steric groups such as (i) diisopropylphenyl and (ii) **NI** units on either side could prevent stronger association of **PI** units in **(*R*)-NP(OH)$_2$**.

^{1}HNMR titration of **(*R*)-NP(OH)$_2$** in CD_2Cl_2 with increase in volume fraction of hexane (0–67%) shows significant upfield shift and broadening in the protons corresponding to the **NI** and **PI** units (Fig. S6†) which indicates hydrophobic interactions between aromatic units that results in the self-assembly of **(*R*)-NP(OH)$_2$** in DCM:hexane mixture. A critical **(*R*)-NP(OH)$_2$** concentration of 1 mM in DCM:hexane (1:2) mixture offered a stable red transparent gel. The d-spacing at 3.7 Å in the **(*R*)-NP(OH)$_2$** xerogel is indicative of the interplanar distance between two adjacent **PI** units through π-π interactions, as evident from powder X-ray diffraction (XRD; Fig. S7†). The broad XRD peaks clearly show less ordered intermolecular close packing arrangement in the gel compared to the sharp peaks observed in the non-gelated powdered **(*R*)-NP(OH)$_2$** solid.[55] Infrared absorption spectra exhibited red-shifted broad peaks at 3432 cm^{-1} (sol-gel) and 3446 cm^{-1} (xerogel) when compared to the sharp peak at 3545 cm^{-1} in the non-gelated solid **(*R*)-NP(OH)$_2$** suggesting intermolecular hydrogen-bonding interactions (Fig. S8†).

Similar results were obtained for the **(*S*)-NP(OH)$_2$** isomer of the dyad. However, **NP(OH)**, **NP(OH)$_3$**, **NP(OAc)$_2$** and **NP(OAc)$_3$** could not gelate under similar conditions implying the role of amphiphilicity and/or chirality imparted by the hydroxypropyl side-chain in **(*R*/*S*)-NP(OH)$_2$** on the formation of the gel. Moreover, **(*R*/*S*)-NP(OH)$_2$** in DCM showed negligible self-aggregation even upto 0.8 mM **(*R*/*S*)-NP(OH)$_2$** as understood from UV–Vis absorbance data (Fig. S5c, d†) indicating the role of DCM/hexane mixture in the formation of dyad based vesicular gel.

Dynamic light scattering (DLS) experiments suggest the formation of spherical particles having an average hydrodynamic diameter of 65 nm and a polydispersity index of 0.17 at 0.01 mM freshly prepared **(*R*)-NP(OH)$_2$** in DCM:hexane (1:2) solution (Fig. 3a; Fig. S9a†). With increase in concentration of **(*R*)-NP(OH)$_2$** (0.01–0.25 mM), a progressive increase in the average diamater of the particles ranging from 65–190 nm indicates the concentration-dependent size distribution of the spherical aggregates (Fig. 3a–e). With the progress of time (~15 min), we observed an initial **(*R*)-NP(OH)$_2$** concentration-dependent increase in the diameter (Fig. S9b†). This reveals aggregation of smaller particles leading to formation of gel at the critical concentration of 1 mM **(*R*)-NP(OH)$_2$**. Initial rate kinetic analysis of the increase in particle size offered first-order rate constant k = 0.03 min^{-1} with respect to the dyad for 0.01 mM **(*R*)-NP(OH)$_2$** (Fig. S10†). At 0.25 mM **(*R*)-NP(OH)$_2$**, we observed a first-order rate constant k = 0.09 min^{-1} implying that rate of particle size growth enhances with increase in initial concentration of **(*R*)-NP(OH)$_2$**.

Atomic force microscopy (AFM) images at different initial concentrations of **(*R*)-NP(OH)$_2$** were recorded. At 0.05 mM **(*R*)-NP(OH)$_2$**, we observed a distribution of spherical particles having an average diameter of 60 nm (Fig. S11a†), consistent with DLS data (Fig. 3f).

As the initial concentration of **(*R*)-NP(OH)$_2$** increased to 0.1 mM, we observed coalescence of spherical particles to form a linear (Fig. 3g) assembly that gels at a higher concentration (Fig. 3h). Scanning electron microscopy (SEM) image of 0.1 mM **(*R*)-NP(OH)$_2$** confirms the formation of regular spherical particles having an average diameter of 160 nm (Fig. 3i; Fig. S11b†). As the concentration increases from 0.01 mM to 0.5 mM **(*R*)-NP(OH)$_2$**, SEM showed fusion of spherical particles leading to the formation of a coalesced assembly of spherical

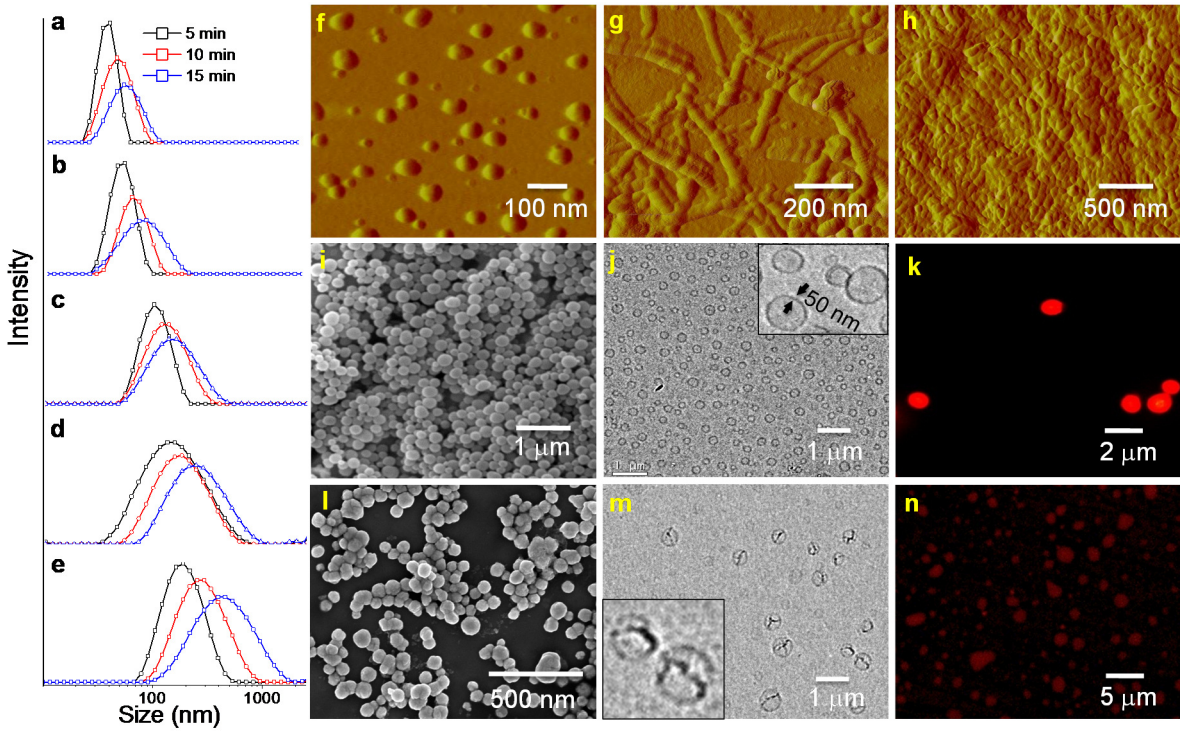

Fig. 3 Dynamic light scattering and microscopic investigation of vesicular scaffold. Time-dependent size distribution of spherical aggregates at (a) 0.01; (b) 0.02; (c) 0.05; (d) 0.1 and (e) 0.25 mM **(*R*)-NP(OH)$_2$** in DCM:hexane (1:2) determined by DLS measurements; Tapping mode AFM images of **(*R*)-NP(OH)$_2$** at (f) 0.05; (g) 0.1 and (h) 0.5 mM (Amplitude image Z Scale = 12.9 (f), 45.8 (g) and 103.1 (h) mV respectively); SEM images of 0.1 mM **(*R*)-NP(OH)$_2$** in the (i) absence and (l) presence of indole (1 mM); and HR-TEM images of 0.25 mM **(*R*)-NP(OH)$_2$** in the (j) absence and (m) presence of indole (2.5 mM); OM images (λ_{ex} = 365 nm) of 0.25 mM **(*R*)-NP(OH)$_2$** in the (k) absence and (n) presence of indole (2.5 mM) in DCM:hexane (1:2) mixture.

aggregates, consistent with AFM data (Fig. S12a-f†). The transmission electron microscopy (TEM) image of 0.25 mM **(*R*)-NP(OH)$_2$** exhibited an average diameter of 260 nm of spherical

particles (Fig. 3j; Fig. S11c†). The observed contrast between the periphery (ca. 50 nm thickness) and the inner part indicate the vesicular nature of the spherical particles. Under similar conditions, bright fluorescent red spheres having an average diameter of 650 nm were visible in the optical microscope (OM) when excited at 365 nm (Fig. 3k).

UV–Vis absorption spectrum of **(*R*)-NP(OH)$_2$** gel exhibited absorbance at 341 nm (**NI**) and 505 nm (**PI**) having a shoulder at 550 nm (Fig. 2a) corresponding to weak **PI** aggregates. **(*R*)-NP(OH)$_2$** thin film exhibited significantly red-shifted (~21 nm) absorbance at 530 nm (**PI**) indicating the presence of strong **PI** aggregates. **(*R*)-NP(OH)$_2$** gel exhibited strong positively induced CD signals at 370 nm and 545 nm corresponding to **NI** and **PI** units, similar to **(*R*)-NP(OH)$_2$** thin film (Fig. 2b). Negatively induced CD signals were obtained for **(*S*)-NP(OH)$_2$** gel and thin film corresponding to **NI** and **PI** units. A strong red-orange fluorescence (Φ_f = 0.54 ± 0.02; λ_{em} = 584 nm) is exhibited by **(*R*)-NP(OH)$_2$** gel, when excited both at 345 nm and 475 nm (Fig. 2c, S3†). Observed spectral narrowing (fwhm = 60 nm) in the emission of **(*R*)-NP(OH)$_2$** gel compared to thin film (fwhm = 130 nm) could be attributed to the re-absorption of photons due to high optical density in the gel state. Upon excitation both at 345 nm and 475 nm, thin film of **(*R*)-NP(OH)$_2$** exhibited a significantly red-shifted (λ_{em} = 625 nm) weak broad fluorescence corresponding to **PI** (Φ_f = 0.05 ± 0.002) consistent with the UV–Vis absorption data.

Picosecond time-resolved fluorescence of **(*R*)-NP(OH)$_2$** gel (Fig. 2d) exhibited bi-exponential decay having lifetimes of 2.9 ns (53%) and 4.7 ns (47%), upon excitation at 340 nm. Similar lifetimes were observed on exciting the perylenimide unit at 439 nm (Fig. S4c, d†). Relatively minor component could be attributed to the slower decay of excimeric **PI** in the dyad **(*R*)-NP(OH)$_2$** gel, while the short-lived component could be attributed to the monomeric **PI**. **(*R*)-NP(OH)$_2$** in DCM exhibited a moderately faster rate of radiative decay (k_r = 1.9 × 10^8 s^{-1})

compared to gel (k_r = 1.4 × 10^8 s^{-1}; see ESI†) which indicates that the **PI** units undergo very weak H-type exciton interactions in the **(*R*)-NP(OH)$_2$** gel, consistent with high-fluorescence quantum yield. **(*R*)-NP(OH)$_2$** thin film showed tri-exponential decay having lifetimes of 3.9 ns (11%), 1.2 ns (34%) and 0.3 ns (55%) upon excitation at 439 nm (Fig. S4e, f†) consistent with the recently reported literature.[56] Tri-exponential and faster radiative decay (k_r = 0.37 × 10^8 s^{-1}) of **(*R*)-NP(OH)$_2$** thin film compared to solution indicates diverse close packing arrangements of **PI** aggregates that possess strong H-type exciton interactions resulting in low Φ_f in thin film.[31]

Time-resolved fluorescence anisotropy of the dyad **(*R*)-NP(OH)$_2$** gel exhibits an initial anisotropy value of 0.17 that loses the anisotropy memory when monitored at 580 nm (**PI** moiety) with a decay time of 201 ps, upon excitation at 439 nm (**PI** unit; Fig. S13†). Ultrafast energy/exciton migration[57, 58] at short separation between the chromophoric transition dipoles predominate over slower fluorescence depolarization through rotational motion at this time-scale in the gel leading to fluorescence anisotropy.[59, 60] A relatively slower rate of energy migration (k_{EM} = 4.97 × 10^9 s^{-1}; λ_{ex} = 439 nm) for **(*R*)-NP(OH)$_2$** gel compared to chromophoric gel assemblies[20] could be attributed to the delayed memory loss arising from the asymmetry of bichromophoric **(*R*)-NP(OH)$_2$**.

Temperature-dependent UV–Vis absorbance of **(*R*)-NP(OH)$_2$** gel exhibited a hypochromism at 550 nm and a concomitant increase in the absorbance at 505 nm (Fig. S14a†) which indicates the dissociation of exciton interactions between the **PI** units at elevated temperature resulting in the destabilisation of gel (T_m = 35°C). With increase in temperature (20–60°C), **(*R*/*S*)-NP(OH)$_2$** gel shows a gradual decrease in the intensity of CD signal at 370 nm and 545 nm (Fig. S15†). Disappearance of the **NI** and **PI** CD signals at elevated temperature indicates destabilisation of the gel through thermal unstacking of **NI** and **PI** units. Upon

excitation at 345 nm and 475 nm, we observed recovery in the fluorescence quantum yield of **(*R*)-NP(OH)$_2$** (Φ_f = 0.65 ± 0.03) at 60°C (Fig. S14b, c†) corresponding to the monomeric **(*R*)-NP(OH)$_2$**. Temperature-dependent time-resolved fluorescence decay of an **(*R*)-NP(OH)$_2$** gel corresponding to **PI** unit, upon excitation at 340 nm exhibited a transformation of bi-exponential decay at 20°C to mono-exponential decay at 60°C (τ = 3.8 ns). Mono-exponential decay of **(*R*)-NP(OH)$_2$** gel at elevated temperature is consistent with the formation of monomeric **(*R*)-NP(OH)$_2$** and the disappearance of self-assembled structure (Fig. S14d†).

Amphiphilic **(*R*)-NP(OH)$_2$** in DCM/hexane mixture at a low concentration forms individual multi-lamellar vesicles that can transform into bigger vesicles with the progression of time. At higher concentrations (above the critical gelator concentration) the individual bilayer vesicles undergo fusion and forms extended superstructured gel. Kinetically stable gel thus formed slowly transforms, through gliding[61] of the dyad, to thermodynamically stable crystal (Table S1†) over a period of 48 hours (Fig. 4). Metastability (Table S2†) of **(*R*)-NP(OH)$_2$** containing vesicular gel encouraged us to investigate the photoinduced processes in the presence of indole (electron donor). **(*R*)-NP(OH)$_2$** gel retained the stability even at 100:1 indole:**(*R*)-NP(OH)$_2$** ratio. SEM image of 0.1 mM **(*R*)-NP(OH)$_2$** in the presence of 1 mM indole exhibited spheroidal particles having an average diameter of 160 nm (Fig. 3l). Observed surface roughness in the spheroidal particles could arise from the adsorption of indole molecules on **(*R*)-NP(OH)$_2$** vesicular surface. TEM image of 0.25 mM **(*R*)-NP(OH)$_2$** in the presence of 2.5 mM indole exhibits spheroidal particles having an average diameter of 400 nm (Fig. 3m). An additional contrast on the vesicular surface, apart from the rim of the spheroidal particles of **(*R*)-NP(OH)$_2$** xerogel, confirms the integrity of vesicles having indole molecules adsorbed on the surface. Optical microscopy image (Fig. 3n) of **(*R*)-NP(OH)$_2$** vesicles containing indole showed a

significant fluorescence quenching indicating the possibility of photoinduced electron transfer process from indole to singlet excited states of the chromophoric units.

With increase in indole concentration, **(*R*)-NP(OH)$_2$** gel shows up to 4-fold decrease in the fluorescence quantum yield and significant decrease in the fluorescence lifetime ($\tau = 0.6$ ns), upon excitation both at 345 nm and 475 nm (Fig. S16†). Stern-Volmer analysis[62] of the steady-

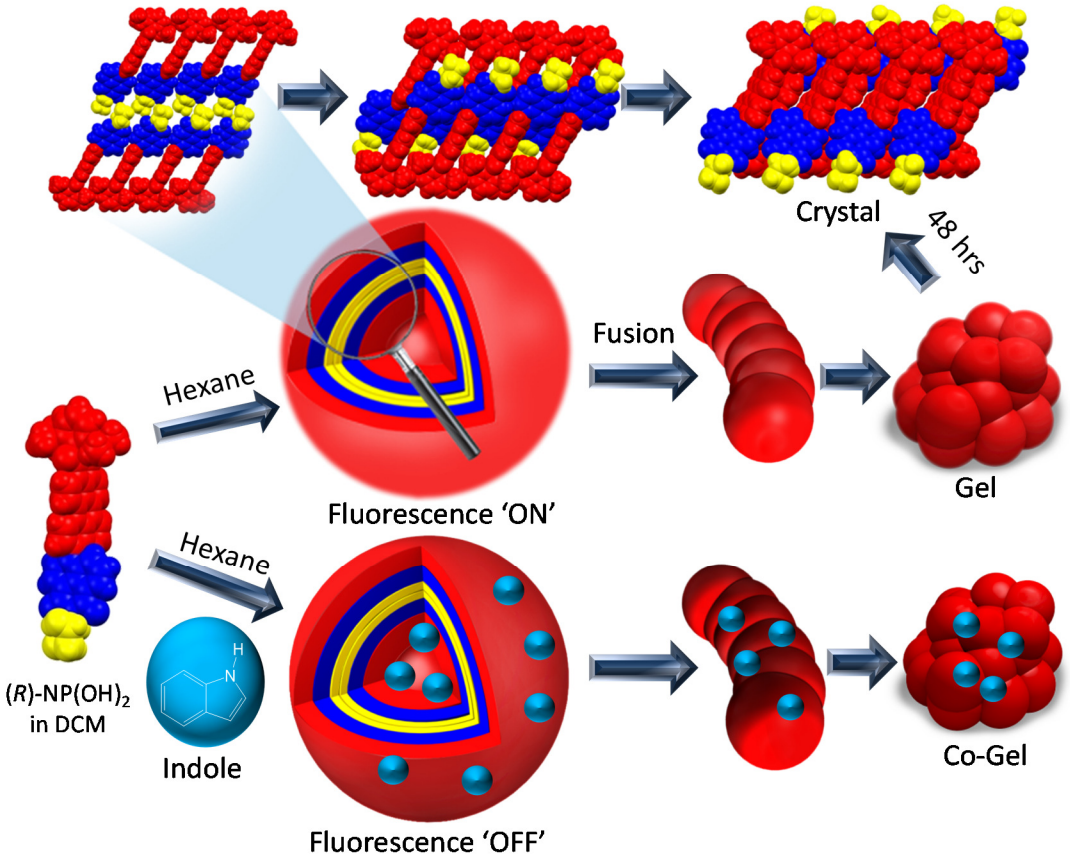

Fig. 4 Mechanism for molecule-bilayer-vesicle-gel-crystal transition. Schematic representation of self-assembly of **(*R*)-NP(OH)$_2$** in DCM:hexane (1:2) mixture in the absence and presence of indole.

state and time-resolved fluorescence data (see ESI†) of **(*R*)-NP(OH)$_2$** gel with increase in concentration of indole offered similar bimolecular quenching rate constant $k_q = 7.2 \times 10^9$ $M^{-1}s^{-1}$ (Fig. S17a-d†) indicating dynamic quenching of singlet excited state of perylenimide (^{1}**PI***). Observed bimolecular quenching rate constant in the case of **(*R*)-NP(OH)$_2$**:indole co-gel is lower

than the upper bound of diffusional bimolecular quenching constant, k_q = 1 × 10^{10} $M^{-1}s^{-1}$ confirming the dynamic nature of photoinduced electron transfer.[63] We observed a similar bimolecular quenching rate constant for the photoinduced electron transfer from indole to the singlet excited state of perylenimide in **(*R*)-NP(OH)$_2$** solution (k_q = 6.2 × 10^9 $M^{-1}s^{-1}$, Fig. S18†) when compared to the co-gel, consistent with D–A pair reported.[64, 65] UV-Vis absorption spectra of the dyad **(*R*)-NP(OH)$_2$** in DCM exhibited negligible change before and after the addition of indole (1000 equivalents) ruling out the possibility of ground state complexation between indole and the constituents of the dyad (Fig. S18a†). Rehm–Weller analysis[66] shows favourable change in free energy for photoinduced electron transfer from the singlet excited state of **NI** to **PI** (–0.17 eV) in the dyad **NP(OH)** as described earlier.[50] Photoinduced electron transfer from indole to the singlet excited state of **NI** (–1.19 eV) and **PI** (–0.48 eV) units (see ESI†) are thermodynamically feasible.

To characterize the transient intermediates generated upon photoexcitation of **(*R*)-NP(OH)$_2$**:indole solution and co-gel, we have carried out femtosecond transient absorption measurements and analysed the three dimensional ΔA versus time and wavelength spectral data using singular value decomposition (SVD). Femtosecond transient absorption (FTA) spectra of 0.75 mM **(*R*)-NP(OH)$_2$** solution exhibited a bleach centered at 570 nm and a mono-exponential decay corresponding to singlet excited state of perylenimide (**^{1}PI***) at 615 nm having a lifetime of 3.1 ns, upon excitation at 390 nm (Fig. S19a,d†). Marginal decrease in the fluorescence quantum yield of **(*R*)-NP(OH)$_2$** (Φ_f = 0.75 ± 0.04) corresponding to **PI** unit when compared to the model perylenimide **PI** derivative (Φ_f = 0.81 ± 0.03) indicates the possibility of photoinduced electron transfer from the singlet excited state of **NI** to **PI** ($\Delta G_{charge\ separation}$ = – 0.17 eV) having an estimated rate of $k_{charge\ separation}$ = 2.29 x 10^{12} s^{-1}.[50] Upon photoexcitation, charge transfer

intermediates in the dyad **(*R*)-NP(OH)$_2$** solution were not observed suggesting the fact that rate of charge recombination (<110 fs) is much faster than the rate of charge separation, consistent with similar reported dyads.[47] In the presence of lower concentration of indole, dyad **(*R*)-NP(OH)$_2$**:indole (1:10) solution exhibited a mono-exponential decay at 617 nm corresponding to ^{1}**PI*** having a lifetime of 2.9 ns, similar to the lifetime of ^{1}**PI*** in the dyad **(*R*)-NP(OH)$_2$** solution (Fig. S19b,e†).[67] Lack of formation of charge transfer intermediates in dyad **(*R*)-NP(OH)$_2$**:indole (1:10) solution is consistent with insignificant fluorescence quenching corresponding to dyad **(*R*)-NP(OH)$_2$** under similar conditions indicating the absence of photoinduced electron transfer from indole to ^{1}**PI***/^{1}**NI***. At a higher concentrations of indole, dyad **(*R*)-NP(OH)$_2$**:indole (1:500 and 1:1000) solution showed a bleach around 570 nm and two absorption bands centered around 598 nm and 619 nm, upon photoexcitation (Fig. 5b, Fig. S19c,f†). SVD analysis followed by global fitting offered a lifetime of 6-6.5 ps at 598 nm corresponding to the radical anion of perylenimide (**PI**$^{\bullet-}$)[48, 68] and 0.5-0.64 ns at 619 nm corresponding to the singlet excited state of perylenimide (^{1}**PI***, inset of Fig. 5b, Table S3†). The formation of charge transfer intermediate **PI**$^{\bullet-}$ in the dyad **(*R*)-NP(OH)$_2$** at higher concentrations of indole (1:500 and 1:1000) solution signifies the occurrence of diffusion controlled photoinduced charge separation[69] that is consistent with the quenching of fluorescence of the dyad **(*R*)-NP(OH)$_2$** (Fig. S18b,d†). Greater dependence on the distribution of charged intermediates with increase in concentration of the electron donor indole indicates that the rate of charge separation dominates over rate of charge recombination (k_{cs}>k_{cr}).[70]

Nanosecond transient absorption spectroscopic measurements of dyad **(*R*)-NP(OH)$_2$**:indole (1:500 and 1:1000) in DCM failed to detect the presence of charged intermediates, upon excitation at 355 nm and 532 nm. Lack of transient intermediates in the

nanosecond transient absorption measurements of the dyad **(*R*)-NP(OH)$_2$**:indole could be attributed to ultrafast charge recombination occurring faster than the time-resolution of the instrument (≥ 10 ns). Observed short lifetime (ca. 6 ps) of the radical anion of perylenimide (**PI**$^{\bullet-}$) from FTA measurements is consistent with the short-lived coumarin-amine based solvent separated radical ion pair (SSRIP) formed through diffusion controlled intermolecular photoinduced electron transfer as reported earlier.[71] Self-assembled vesicular architecture in the dyad **(*R*)-NP(OH)$_2$** gel exhibits a similar monoexponential decay of ^{1}**PI*** (τ=2.9 ns; Fig. 5a and inset of 5a for singular vector) at 620 nm upon photoexcitation. In contrast to an extension in the photoinduced charge separation lifetimes of an assembled guanine-perylenediimide G-quadruplex structure[47] and melamine-perylenimide based foldamer[48] reported by Wasielewski and co-workers, absence of charge transfer intermediates in the dyad **(*R*)-NP(OH)$_2$** gel could be attributed to ultrafast charge recombination of **PI**$^{\bullet-}$ and **NI**$^{\bullet+}$ in <110 fs.

SVD analysis followed by global fitting of FTA spectra of dyad **(*R*)-NP(OH)$_2$**:indole (1:10) co-gel (Fig. 5c) yielded three principal components of the spectra as illustrated in Fig. 5d. The three principal components obtained from SVD could be assigned as the following: i) radical anion of perylenimide (**PI**$^{\bullet-}$)[48, 68] and/or radical cation of indole (**I**$^{\bullet+}$) centered at 597 nm having a lifetime of 2.1 ps,[72, 73] ii) singlet excited state of perylenimide (^{1}**PI***)[67, 74] featured at 620 nm with a lifetime of 3.0 ns and iii) radical anion of π-π stacked perylenimide (π-π **PI**$^{\bullet-}$) at 640 nm having a lifetime of 1.4 ns.[48] We observed a time-dependent shift in the peak corresponding to the decay of **PI**$^{\bullet-}$ indicating the evolution of radical anion of larger π-π stacks of perylenimide (Fig. 5c).[48, 75] Increase in the survival time of **PI**$^{\bullet-}$ in dyad **(*R*)-NP(OH)$_2$**:indole co-gel indicates sequential electron transfer from singlet excited state of naphthalimide (^{1}**NI***) to **PI** followed by an electron transfer from indole to **NI**$^{\bullet+}$, upon excitation of **NI** unit. Alternatively, ^{1}**PI*** formed via energy

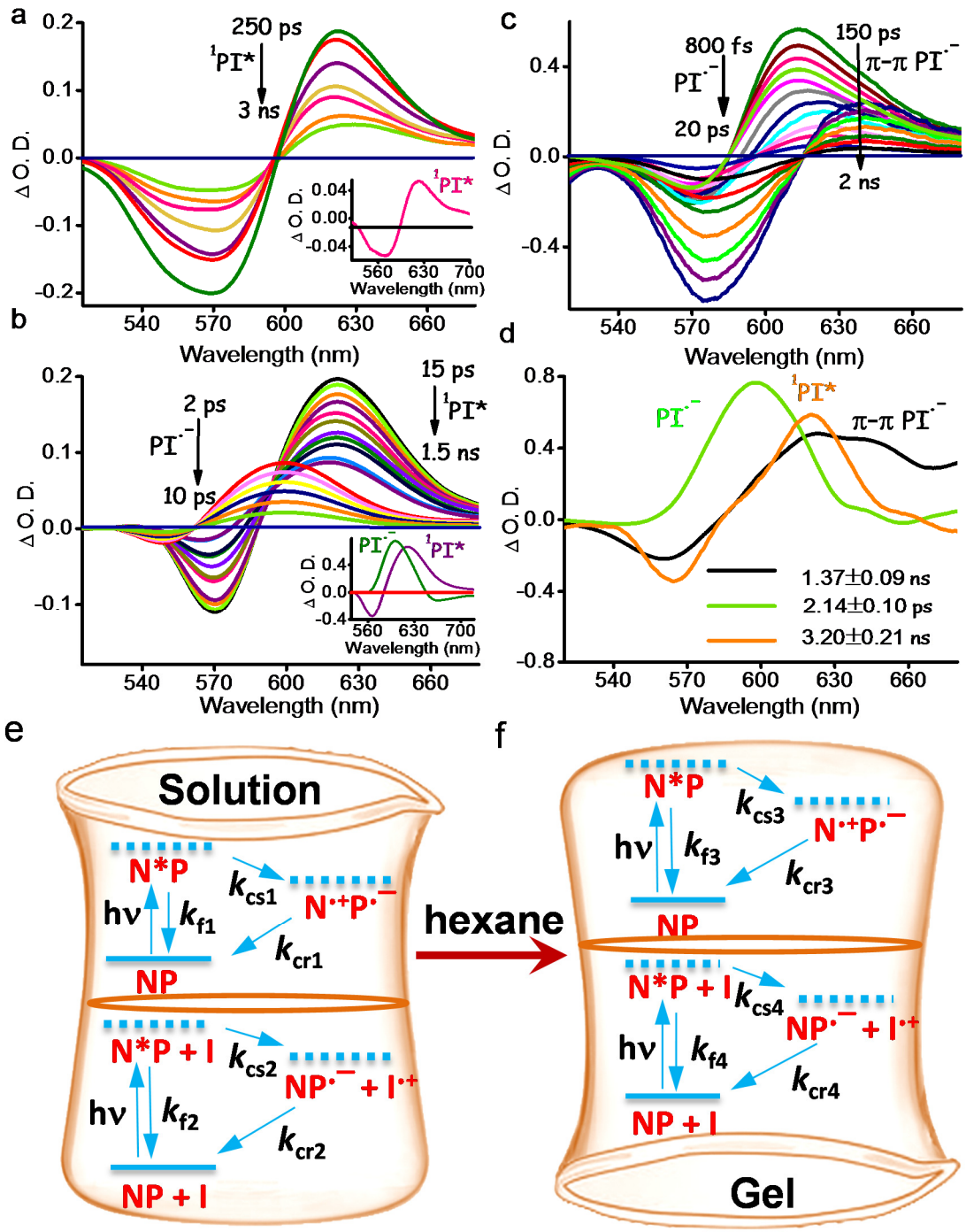

Fig. 5 Ultrafast kinetics and Jablonski diagram showing reduced rate of charge recombination in (***R***)-**NP(OH)$_2$**:indole co-gel. Femtosecond transient absorption (ΔOD) spectra of (a) (***R***)-**NP(OH)$_2$** gel, inset shows the principal component of the spectra obtained from SVD; (b) (***R***)-**NP(OH)$_2$** solution in presence of 1000 equivalents of indole in DCM, inset of (b) shows the prinicipal components of the spectra obtained from SVD; (c) (***R***)-**NP(OH)$_2$**:indole co-gel excited at 390 nm; (d) principal components of the spectra shown in (c) from SVD; Jablonski diagram of the (***R***)-**NP(OH)$_2$** in the absence and presence of indole (**I**) in (e) solution and (f) gel.

transfer from ^{1}**NI*** can abstract an electron from indole leading to the formation of **PI**$^{\bullet-}$ and radical cation of indole. Lifetime of **PI**$^{\bullet-}$ is found to be comparable in the dyad **(*R*)-NP(OH)$_2$**:indole (1:10) co-gel and in the dyad **(*R*)-NP(OH)$_2$**:indole (1:1000) solution indicating photoinduced charge separation followed by fast charge recombination (ca. 2-6 ps). While longer survival time of the charge transfer intermediate arising from π-π **PI**$^{\bullet-}$ (ca. 1.4 ns) in the dyad **(*R*)-NP(OH)$_2$**:indole (1:10) co-gel, which is absent in the dyad **(*R*)-NP(OH)$_2$**:indole (1:1000) solution, could be attributed to the favourable supramolecular arrangement of the donor-acceptor systems for efficient charge separation followed by slow charge recombination. A remarkable increase in survival time of π-π **PI**$^{\bullet-}$ in **(*R*)-NP(OH)$_2$** gel (Fig. 5c,f) *vs.* solution (Fig. 5e) in the presence of indole could be attributed to the decrease in the rate of diffusion of transient intermediates in highly viscous medium (gel) resulting in slower rate of charge recombination (k_{cr4}) compared to the solution (k_{cr2}), as reported in the self-assembled systems.[39, 76]

Jablonski diagram in Fig. 5e, f demonstrates competitive deactivation pathways of the singlet excited state via fluorescence and electron transfer states of the dyad **(*R*)-NP(OH)$_2$** upon photoexcitation under different conditions. Analysis of time-resolved fluorescence and femtosecond transient spectroscopic data revealed that $k_{cs1,3} <<< k_{cr1,3}$ respectively and hence intrinsic fluorescence decay predominates over charge separation in **(*R*)-NP(OH)$_2$** solution/gel. At lower concentration of indole, **(*R*)-NP(OH)$_2$** in DCM exhibited negligible decrease in the fluorescence quantum yield indicating the lack of forward electron transfer from indole to ^{1}**PI***/^{1}**NI*** through bimolecular process (k_q[M]<<k_f; Table S3†). At higher concentrations of indole, rate of bimolecular quenching is comparable to the rate of fluorescence (k_q[M]≈k_f; Table S3†) resulting in efficient photoinduced electron transfer from indole to ^{1}**PI***/^{1}**NI***. While in the case of **(*R*)-NP(OH)$_2$**:indole co-gel (1:10), rate of bimolecular quenching could compete with the

intrinsic decay of the singlet excited state thereby resulting in efficient photoinduced charge separation (k_q[M]≈k_f; Table S3†) followed by slow charge recombination (k_{cr}<<k_{cs}; Table S3†). A significant decrease in the rate of charge recombination could be a consequence of the extended charge delocalisation through supramolecular π-π stacked arrangement of perylenimide units in **(*R*)-NP(OH)$_2$**:indole co-gel.

Conclusions

In summary, the amphiphilic nature offered by the chiral side-chain (lyophobic) and orthogonal naphthalimide-perylenimide unit (lyophilic) in **(*R/S*)-NP(OH)$_2$** in DCM forces the molecules to form bilayer vesicle with an increase in volume fraction of hexane. We observed growth of the vesicles followed by fusion to form superstructured gel with increase in concentration of the dyad **(*R/S*)-NP(OH)$_2$** and progress of time. The metastable nature of gel forces the dyad **(*R/S*)-NP(OH)$_2$** to undergo gliding resulting in thermodynamically stable crystal. Highly efficient energy transfer from naphthalimide to perylenimide unit upon excitation at 345 nm and direct excitation of perylenimide unit (λ_{ex} = 475 nm) in the vesicular gel makes this dyad **(*R/S*)-NP(OH)$_2$** an excellent light-harvesting assembly. Upon photoexcitation, a remarkable decrease in the rate of charge recombination of transient intermediates in **(*R/S*)-NP(OH)$_2$** gel, in the presence of an electron-donor when compared to **(*R/S*)-NP(OH)$_2$**:indole solution, is observed. Enhanced survival time of the radical intermediates in the **(*R/S*)-NP(OH)$_2$**:indole co-gel is an effect of favourable supramolecular arrangement that stabilises the radical anion of perylenimide in π-π stacked self-assembled structure of **(*R/S*)-NP(OH)$_2$**, a feature that is inaccessible in non-assembled D-A systems based photoinduced charge separation. Sequential photoinduced energy/electron transfer processes followed by delayed charge-recombination in solution

processable self-assembled donor-acceptor arrays are essential for the fabrication of photovoltaic devices and artificial photosynthesis.

Acknowledgment

Authors dedicate this work to Professor Frederick D. Lewis on the occasion of his 70th Birthday. M. H. acknowledges the Science and Engineering Research Board, SERB/F/0962 for the financial support of this work. Authors acknowledge Dr. Reji Varghese, Dr. Anil Shaji, Mr. K. Nagarajan, IISER-TVM and Dr. C. S. Rajesh for helpful discussion and CSIR-NIIST-Thiruvananthapuram for microscopy measurements. Authors gratefully acknowledge the anonymous reviewers for their valuable comments and suggestions to improve the quality of the manuscript.

Notes and references

1. H. V. Amerongen, L. Valkunas and R. V. Grondelle, *Photosynthetic Excitons*, World Scientific, London, 2000.
2. G. S. Engel, T. R. Calhoun, E. L. Read, T.-K. Ahn, T. Mancal, Y.-C. Cheng, R. E. Blankenship and G. R. Fleming, *Nature*, 2007, **446**, 782-786.
3. A. K. Ringsmuth, G. J. Milburn and T. M. Stace, *Nat. Phys.*, 2012, **8**, 562-567.
4. G. D. Scholes, *J. Phys. Chem. Lett.*, 2010, **1**, 2-8.
5. Y. Tachibana, L. Vayssieres and J. R. Durrant, *Nature Photon.*, 2012, **6**, 511-518.
6. D. G. Nocera, *Acc. Chem. Res.*, 2012, **45**, 767-776.
7. D. Gust, T. A. Moore and A. L. Moore, *Acc. Chem. Res.*, 2009, **42**, 1890-1898.
8. A. A. Bakulin, S. D. Dimitrov, A. Rao, P. C. Y. Chow, C. B. Nielsen, B. C. Schroeder, I. McCulloch, H. J. Bakker, J. R. Durrant and R. H. Friend, *J. Phys. Chem. Lett.*, 2012, **4**, 209-215.
9. Y. Sun, N. C. Giebink, H. Kanno, B. Ma, M. E. Thompson and S. R. Forrest, *Nature*, 2006, **440**, 908-912.
10. T. Aida, E. W. Meijer and S. I. Stupp, *Science*, 2012, **335**, 813-817.
11. V. Coropceanu, J. Cornil, D. A. da Silva Filho, Y. Olivier, R. Silbey and J.-L. Brédas, *Chem. Rev.*, 2007, **107**, 926-952.
12. Z. B. Henson, K. Mullen and G. C. Bazan, *Nat. Chem.*, 2012, **4**, 699-704.
13. M. E. El-Khouly, C. A. Wijesinghe, V. N. Nesterov, M. E. Zandler, S. Fukuzumi and F. D'Souza, *Chem.–Eur. J.*, 2012, **18**, 13844-13853.
14. J. Kim, D. T. McQuade, A. Rose, Z. Zhu and T. M. Swager, *J. Am. Chem. Soc.*, 2001, **123**, 11488-11489.

15. F. J. M. Hoeben, I. O. Shklyarevskiy, M. J. Pouderoijen, H. Engelkamp, A. P. H. J. Schenning, P. C. M. Christianen, J. C. Maan and E. W. Meijer, *Angew. Chem. Int. Ed.*, 2006, **45**, 1232-1236.
16. X. Zhang, S. Rehm, M. M. Safont-Sempere and F. Würthner, *Nat. Chem.*, 2009, **1**, 623-629.
17. N. Sakai and S. Matile, *Nat. Chem.*, 2009, **1**, 599-600.
18. K.-P. Tseng, F.-C. Fang, J.-J. Shyue, K.-T. Wong, G. Raffy, A. Del Guerzo and D. M. Bassani, *Angew. Chem. Int. Ed.*, 2011, **50**, 7032-7036.
19. A. Ajayaghosh, S. J. George and V. K. Praveen, *Angew. Chem. Int. Ed.*, 2003, **42**, 332-335.
20. A. Ajayaghosh, V. K. Praveen, C. Vijayakumar and S. J. George, *Angew. Chem. Int. Ed.*, 2007, **46**, 6260-6265.
21. C. Vijayakumar, V. K. Praveen and A. Ajayaghosh, *Adv. Mater.*, 2009, **21**, 2059-2063.
22. K. Sugiyasu, N. Fujita and S. Shinkai, *Angew. Chem. Int. Ed.*, 2004, **43**, 1229-1233.
23. D. Markovitsi, A. Germain, P. Millie, P. Lecuyer, L. Gallos, P. Argyrakis, H. Bengs and H. Ringsdorf, *J. Phys. Chem.*, 1995, **99**, 1005-1017.
24. R. C. Powell and R. G. Kepler, *Mol. Cryst. Liq. Cryst.*, 1970, **11**, 349-360.
25. C. Giansante, G. Raffy, C. Schäfer, H. Rahma, M.-T. Kao, A. G. L. Olive and A. Del Guerzo, *J. Am. Chem. Soc.*, 2010, **133**, 316-325.
26. X. Zhang, Z. Chen and F. Würthner, *J. Am. Chem. Soc.*, 2007, **129**, 4886-4887.
27. A. C. Benniston, G. Copley, A. Harriman, D. B. Rewinska, R. W. Harrington and W. Clegg, *J. Am. Chem. Soc.*, 2008, **130**, 7174-7175.
28. H. Tian, P.-H. Liu, W. Zhu, E. Gao, D.-J. Wu and S. Cai, *J. Mater. Chem.*, 2000, **10**, 2708-2715.
29. L. Le Pleux, A. L. Smeigh, E. Gibson, Y. Pellegrin, E. Blart, G. Boschloo, A. Hagfeldt, L. Hammarstrom and F. Odobel, *Energy Environ. Sci.*, 2011, **4**, 2075-2084.
30. S. Leroy-Lhez, J. Baffreau, L. Perrin, E. Levillain, M. Allain, M.-J. Blesa and P. Hudhomme, *J. Org. Chem.*, 2005, **70**, 6313-6320.
31. R. T. Cheriya, K. Nagarajan and M. Hariharan, *J. Phys. Chem. C*, 2013, **117**, 3240-3248.
32. J.-H. Olivier, J. Barberá, E. Bahaidarah, A. Harriman and R. Ziessel, *J. Am. Chem. Soc.*, 2012, **134**, 6100-6103.
33. D. Görl, X. Zhang and F. Würthner, *Angew. Chem. Int. Ed.*, 2012, **51**, 6328-6348.
34. Z. Zhang, C. Zhan, X. Zhang, S. Zhang, J. Huang, A. D. Q. Li and J. Yao, *Chem.–Eur. J.*, 2012, **18**, 12305-12313.
35. J. A. Foster, M. PiepenbrockMarc-Oliver, G. O. Lloyd, N. Clarke, A. K. HowardJudith and J. W. Steed, *Nat Chem.*, 2010, **2**, 1037-1043.
36. M. Shimizu and T. Hiyama, *Chem. Asian J.*, 2010, **5**, 1516-1531.
37. N. S. S. Kumar, S. Varghese, G. Narayan and S. Das, *Angew. Chem. Int. Ed.*, 2006, **45**, 6317-6321.
38. S. Yagai, M. Ishii, T. Karatsu and A. Kitamura, *Angew. Chem. Int. Ed.*, 2007, **46**, 8005-8009.
39. Y. Yamamoto, T. Fukushima, Y. Suna, N. Ishii, A. Saeki, S. Seki, S. Tagawa, M. Taniguchi, T. Kawai and T. Aida, *Science*, 2006, **314**, 1761-1764.
40. M. R. Wasielewski, *Chem. Rev.*, 1992, **92**, 435-461.
41. B. Rybtchinski, L. E. Sinks and M. R. Wasielewski, *J. Am. Chem. Soc.*, 2004, **126**, 12268-12269.
42. M. R. Wasielewski, *Acc. Chem. Res.*, 2009, **42**, 1910-1921.
43. J. Strümpfer, M. Şener and K. Schulten, *J. Phys. Chem. Lett.*, 2012, **3**, 536-542.

44. G. Steinberg-Yfrach, P. A. Liddell, S.-C. Hung, A. L. Moore, D. Gust and T. A. Moore, *Nature*, 1997, **385**, 239-241.
45. F. J. M. Hoeben, P. Jonkheijm, E. W. Meijer and A. P. H. J. Schenning, *Chem. Rev.*, 2005, **105**, 1491-1546.
46. M. K. Şener, J. D. Olsen, C. N. Hunter and K. Schulten, *Proc. Natl. Acad. Sci. USA*, 2007, **104**, 15723-15728.
47. Y.-L. Wu, K. E. Brown and M. R. Wasielewski, *J. Am. Chem. Soc.*, 2013, **135**, 13322-13325.
48. K. M. Lefler, D. T. Co and M. R. Wasielewski, *J. Phys. Chem. Lett.*, 2012, **3**, 3798-3805.
49. B. Grimm, J. Schornbaum, H. Jasch, O. Trukhina, F. Wessendorf, A. Hirsch, T. Torres and D. M. Guldi, *Proc. Natl. Acad. Sci. USA*, 2012, **109**, 15565-15571.
50. R. T. Cheriya, J. Joy, A. P. Alex, A. Shaji and M. Hariharan, *J. Phys. Chem. C*, 2012, **116**, 12489-12498.
51. R. T. Cheriya, J. Joy, S. K. Rajagopal, K. Nagarajan and M. Hariharan, *J. Phys. Chem. C*, 2012, **116**, 22631-22636.
52. K. Mislow, *Angew. Chem.*, 1958, **70**, 683-689.
53. J. Joy, R. T. Cheriya, K. Nagarajan, A. Shaji and M. Hariharan, *J. Phys. Chem. C*, 2013, **117**, 17927-17939.
54. Transition density cube analysis offered a strong Coulombic coupling (V_{ET} = 3.5 cm^{-1}) and a rate of energy transfer k_{ET} = 2.2 x 10^{10} s^{-1} for a dihedral angle of 75° and a separation distance of 1.49 Å between the two constituent chromophoric units.
55. E. Ostuni, P. Kamaras and R. G. Weiss, *Angew. Chem. Int. Ed.*, 1996, **35**, 1324-1326.
56. S. W. Eaton, L. E. Shoer, S. D. Karlen, S. M. Dyar, E. A. Margulies, B. S. Veldkamp, C. Ramanan, D. A. Hartzler, S. Savikhin, T. J. Marks and M. R. Wasielewski, *J. Am. Chem. Soc.*, 2013, **135**, 14701–14712.
57. Exciton migration within the dyad **(*R*)-NP(OH)$_2$** in the aggregated state leads to a loss of the memory of the initial excitation polarization, thereby resulting in equal intensities of the polarized emitted light that is either parallel or perpendicular to the polarisation of the excitation source; Refer: L. M. Herz et al., *Phys. Rev. B* 2003, **68**, 045203-045209.
58. J.-S. Yang, J.-L. Yan, C.-Y. Hwang, S.-Y. Chiou, K.-L. Liau, H.-H. Gavin Tsai, G.-H. Lee and S.-M. Peng, *J. Am. Chem. Soc.*, 2006, **128**, 14109-14119.
59. A. El-ghayoury, A. P. H. J. Schenning, P. A. van Hal, J. K. J. van Duren, R. A. J. Janssen and E. W. Meijer, *Angew. Chem. Int. Ed.*, 2001, **40**, 3660-3663.
60. A. Sassella, A. Borghesi, F. Meinardi, R. Tubino, M. Gurioli, C. Botta, W. Porzio and G. Barbarella, *Phys. Rev. B*, 2000, **62**, 11170-11176.
61. J. Cui, Z. Shen and X. Wan, *Langmuir*, 2009, **26**, 97-103.
62. O. Stern and M. Volmer, *Physik. Z.*, 1919, **20**, 183-188.
63. J. R. Lakowicz, *Principles of Fluorescence Spectroscopy*, Springer, New York, 2006.
64. F. Galindo, M. Isabel Burguete, R. Gavara and S. V. Luis, *J. Photochem. Photobiol. A: Chem*, 2006, **178**, 57-61.
65. S. S. Babu, K. K. Kartha and A. Ajayaghosh, *J. Phys. Chem. Lett.*, 2010, **1**, 3413-3424.
66. D. Rehm and A. Weller, *Ber. Bunsenges. Physik. Chem.*, 1969, **73**, 834-839.
67. F. Odobel, M. Séverac, Y. Pellegrin, E. Blart, C. Fosse, C. Cannizzo, C. R. Mayer, K. J. Elliott and A. Harriman, *Chem.–Eur. J.*, 2009, **15**, 3130-3138.
68. J. Boixel, E. Blart, Y. Pellegrin, F. Odobel, N. Perin, C. Chiorboli, S. Fracasso, M. Ravaglia and F. Scandola, *Chem.–Eur. J.*, 2010, **16**, 9140-9153.

69. I. R. Gould and S. Farid, *J. Am. Chem. Soc.*, 1993, **115**, 4814-4822.
70. R. C. Dorfman, Y. Lin and M. D. Fayer, *J. Phys. Chem.*, 1989, **93**, 6388-6396.
71. S. Nad and H. Pal, *J. Phys. Chem. A*, 1999, **104**, 673-680.
72. J. Peon, G. C. Hess, J.-M. L. Pecourt, T. Yuzawa and B. Kohler, *J. Phys. Chem. A*, 1999, **103**, 2460-2466.
73. Y.-T. Kao, X. Guo, Y. Yang, Z. Liu, A. Hassanali, Q.-H. Song, L. Wang and D. Zhong, *J. Phys. Chem. B*, 2012, **116**, 9130-9140.
74. A. Petrella, J. Cremer, L. De Cola, P. Bäuerle and R. M. Williams, *J. Phys. Chem. A*, 2005, **109**, 11687-11695.
75. M. Lor, S. Jordens, G. De Belder, G. Schweitzer, E. Fron, L. Viaene, M. Cotlet, T. Weil, K. Mullen, J. W. Verhoeven, M. Van der Auweraer and F. C. De Schryver, *Photochem. Photobiol. Sci.*, 2003, **2**, 501-510.
76. M. R. Wasielewski, *J. Org. Chem.*, 2006, **71**, 5051-5066.

Table of Contents: Graphical Abstract

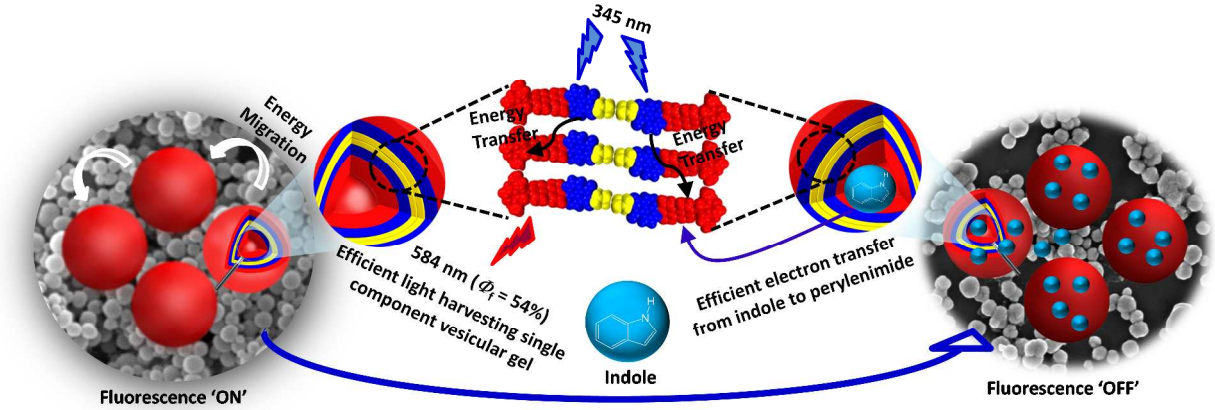

This work highlights the utility of π-π stacked self-assembly for enhanced survival time of charge transfer intermediates upon photoexcitation of donor-acceptor systems.